Experimental study of low-loss single-mode performance in anti-resonant hollow-core fibers

Fei Yu,* Mengrong Xu, and Jonathan C. Knight

Centre for Photonics and Photonic Materials, Department of Physics, University of Bath, Bath, BA2 7AY, UK
**fy230@bath.ac.uk*

Abstract: Anti-resonant hollow-core fibers are optical fiber waveguides which exhibit very low dispersion, high damage threshold and ultra-low nonlinear response. However, they typically deliver the light in several spatial modes, whereas their application usually requires that they support a single spatial mode. We report the principles, fabrication, demonstration and characterization of anti-resonant hollow-core fibres with strong differential modal attenuations and low overall attenuations. These fibers perform as single-mode and are eminently suitable for delivery of powerful ultrashort optical pulses in machining, cutting, welding and multiphoton microscopy applications.

OCIS codes: (060.2280) Fiber design and fabrication; (060.4005) Microstructured fibers; (060.2390) Fiber optics, infrared.

References and links

1. A. D. Pryamikov, A. S. Biriukov, A. F. Kosolapov, V. G. Plotnichenko, S. L. Semjonov, and E. M. Dianov, "Demonstration of a waveguide regime for a silica hollow--core microstructured optical fiber with a negative curvature of the core boundary in the spectral region > 3.5 μm," Opt. Express **19**(2), 1441–1448 (2011).
2. F. Yu, W. J. Wadsworth, and J. C. Knight, "Low loss silica hollow core fibers for 3-4 μm spectral region," Opt. Express **20**(10), 11153–11158 (2012).
3. W. Belardi and J. C. Knight, "Hollow antiresonant fibers with reduced attenuation," Opt. Lett. **39**(7), 1853–1856 (2014).
4. F. Yu and J. Knight, "Negative curvature hollow core optical fiber," IEEE J. Sel. Top. Quantum Electron. **22**(2), 4400610 (2016).
5. N. M. Litchinitser, A. K. Abeeluck, C. Headley, and B. J. Eggleton, "Antiresonant reflecting photonic crystal optical waveguides," Opt. Lett. **27**(18), 1592–1594 (2002).
6. A. Argyros, S. G. Leon-Saval, J. Pla, and A. Docherty, "Antiresonant reflection and inhibited coupling in hollow-core square lattice optical fibres," Opt. Express **16**(8), 5642–5648 (2008).
7. P. Jaworski, F. Yu, R. R. J. Maier, W. J. Wadsworth, J. C. Knight, J. D. Shephard, and D. P. Hand, "Picosecond and nanosecond pulse delivery through a hollow-core Negative Curvature Fiber for micro-machining applications," Opt. Express **21**(19), 22742–22753 (2013).
8. P. Jaworski, F. Yu, R. M. Carter, J. C. Knight, J. D. Shephard, and D. P. Hand, "High energy green nanosecond and picosecond pulse delivery through a negative curvature fiber for precision micro-machining," Opt. Express **23**(7), 8498–8506 (2015).
9. J. D. Shephard, A. Urich, R. M. Carter, P. Jaworski, R. R. J. Maier, W. Belardi, F. Yu, W. J. Wadsworth, J. C. Knight, and D. P. Hand, "Silica hollow core microstructured fibers for beam delivery in industrial and medical applications," Front. Phys. **3**, 24 (2015).
10. M. Michieletto, J. K. Lyngsø, C. Jakobsen, J. Lægsgaard, O. Bang, T. T. Alkeskjold, O. Bang, and T. T. Alkeskjold, "Hollow-core fibers for high power pulse delivery," Opt. Express **24**(7), 7103–7119 (2016).
11. K. Saitoh, N. J. Florous, T. Murao, and M. Koshiba, "Design of photonic band gap fibers with suppressed higher-order modes: towards the development of effectively single mode large hollow-core fiber platforms," Opt. Express **14**(16), 7342–7352 (2006).
12. J. M. Fini, "Aircore microstructure fibers with suppressed higher-order modes," Opt. Express **14**(23), 11354–11361 (2006).
13. J. M. Fini, J. W. Nicholson, R. S. Windeler, E. M. Monberg, L. Meng, B. Mangan, A. Desantolo, and F. V. DiMarcello, "Low-loss hollow-core fibers with improved single-modedness," Opt. Express **21**(5), 6233–6242 (2013).
14. L. Vincetti and V. Setti, "Waveguiding mechanism in tube lattice fibers," Opt. Express **18**(22), 23133–23146 (2010).

#262357 Received 7 Apr 2016; revised 20 May 2016; accepted 27 May 2016; published 6 Jun 2016

15. C. Wei, R. A. Kuis, F. Chenard, C. R. Menyuk, and J. Hu, "Higher-order mode suppression in chalcogenide negative curvature fibers," Opt. Express **23**(12), 15824–15832 (2015).
16. M. C. Günendi, P. Uebel, M. H. Frosz, and P. S. J. Russell, "Broad-band robustly single-mode hollow-core PCF by resonant filtering of higher order modes," arXiv. **1448**(2011), 11153–11158 (2015).
17. P. Uebel, M. Günendi, M. H. Frosz, G. Ahmed, N. Edavalath, J.-M. Ménard, and P. S. Russell, "A broad-band robustly single-mode hollow-core PCF by resonant filtering of higher order modes," in *Frontiers in Optics 2015*, OSA Technical Digest (online) (Optical Society of America, 2015), paper FW6C.2.
18. J. R. Hayes, S. R. Sandoghchi, T. D. Bradley, Z. Liu, R. Slavik, M. A. Gouveia, N. V. Wheeler, G. T. Jasion, Y. Chen, E. Numkam-Fokoua, M. N. Petrovich, D. J. Richardson, and F. Poletti, "Antiresonant hollow core fiber with octave spanning bandwidth for short haul data communications," in *Optical Fiber Communication Conference* Postdeadline Papers, OSA Technical Digest (online) (Optical Society of America, 2016), paper Th5A.3.
19. E. Marcatili and R. Schmeltzer, "Hollow metallic and dielectric waveguides for long distance optical transmission and lasers," Bell Syst. Tech. J. **43**(4), 1783–1809 (1964).
20. C. Harvey, F. Yu, J. C. Knight, W. Wadsworth, and P. Almeida, "Reducing nonlinear limitations of Ytterbium mode-locked fibre lasers with hollow-core negative curvature fibre," in *CLEO: 2015*, OSA Technical Digest (online) (Optical Society of America, 2015), paper STh1L.5.
21. J. W. Nicholson, A. D. Yablon, S. Ramachandran, and S. Ghalmi, "Spatially and spectrally resolved imaging of modal content in large-mode-area fibers," Opt. Express **16**(10), 7233–7243 (2008).
22. J. W. Nicholson, L. Meng, J. M. Fini, R. S. Windeler, A. DeSantolo, E. Monberg, F. DiMarcello, Y. Dulashko, M. Hassan, and R. Ortiz, "Measuring higher-order modes in a low-loss, hollow-core, photonic-bandgap fiber," Opt. Express **20**(18), 20494–20505 (2012).
23. http://doi.org/10.15125/BATH-00189

1. Introduction

Anti-resonant hollow-core optical fibers (AR-HCFs) are a form of microstructured fiber in which light is trapped in the hollow core by a microstructured cladding material [1–4]. The confinement mechanism of AR-HCFs is reflection from a thin glass core wall which functions like a Fabry-Perot resonator [5, 6]. At anti-resonant wavelengths leakage from the core is thus substantially reduced, giving attenuations as low as a few tens of dB/km [4]. The fact that the light propagates in a large hollow (or, typically, air-filled) core confers favourable properties on the fiber, namely a high damage threshold, very low dispersion and ultra-low nonlinear response. As a result, AR-HCFs are outstanding candidates for applications which demand delivery of powerful picosecond and sub-picosecond optical pulses over lengths of a few to a few tens of meters [7–10], where conventional optical fibers are simply not up to the task.

However, higher-order mode suppression in transmission through short lengths of AR-HCFs is a major challenge. In AR-HCFs, no mode cut-off condition exists and all modes propagate although with different attenuations. The existence of higher-order core modes degrades the beam quality at the fiber output and reduces its utility for many applications.

Previous investigations of single-mode guidance of hollow-core fibers have included the study of photonic bandgap hollow-core fiber (PBG-HCF) [11,12]. The coupling between higher-order modes of the core and fundamental modes of ancillary shunt cores embedded in the cladding is optimized by phase matching [13].

In comparison with PBG-HCFs, AR-HCFs are characterized by their much simpler cladding structures [4], which leaves us some flexibility in cladding design for higher-order mode suppression. In 2010, Vincetti and Setti studied the stripping of higher-order mode propagation using different designs of cladding of AR-HCFs [14]. In 2015, Wei et al discussed using the cladding itself instead of introducing extra defects to achieve specific TE_{01} mode suppression in AR-HCF [15]. Later, Günendi et al predicted broad-band single-mode guidance in AR-HCF by introducing a 6-capilllary cladding design [16]. Later, they experimentally demonstrated the single mode guidance of 57 cm piece of 6 capillary AR-HCF but with an attenuation around 0.18 dB/m at 1.6 μm [17], which might be acceptable for some applications but is a lot higher than the state of the art. During the course of this work, Michieletto et al numerically demonstrated the advantage of 7 capillary cladding design of AR-HCF in higher-order mode suppression [10]. However, in the experimental work in that paper the suppression of LP_{11} and other higher-order modes could only be achieved by introducing bending because the fabricated fiber cross section did not sufficiently match the desired specification for LP_{11} mode stripping. The multimode transmission property was

#262357 Received 7 Apr 2016; revised 20 May 2016; accepted 27 May 2016; published 6 Jun 2016

confirmed in a similar 7 capillary cladding AR-HCF recently and an over octave transmission spectral window was reported [18]. The challenge we have addressed in this work is of robust fundamental-mode beam delivery in a hollow core with state-of-the-art optical attenuation, without relying on fiber bending.

One of the difficulties in implementing proposed designs of AR-HCFs [10, 17, 18] is fine tuning the cladding structure for precise phase matching between the core and cladding modes. Stripping the LP_{11} mode is particularly important because yet higher-order core modes are less likely to be excited and will naturally have higher attenuation rates. In this paper, we experimentally demonstrate broad-band low-loss single-mode performance centered at 1 μm wavelength. LP_{11}-mode-free transmission over 10m length was verified by S^2 characterisation. In transmission through shorter (e.g. 2 m) lengths, LP_{21}-like mode was confirmed with about 2 dB/m attenuation, nearly 100 times higher than for the LP_{01} mode. By scaling this design for other wavelengths, low-loss single-mode performance is also reported at visible wavelengths.

2. Fiber design and fabrication

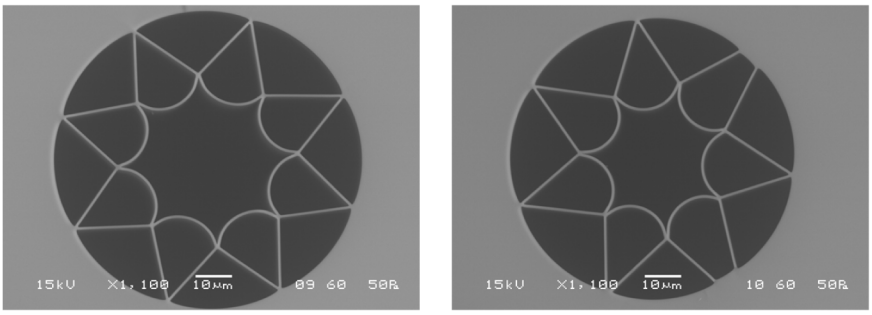

Fig. 1. Scanning electron microscope images of AR-HCFs designed and fabricated with low loss transmission bands centred at 1 μm. ***Left***: AR-HCF of 8 capillary cladding design. The inscribed diameter of core region is about 36 μm. ***Right***: AR-HCF of new 7 capillary cladding design. Fitting an ellipse to the core region, we find long and short axes of 28 μm and 25.5 μm.

The design principle we have used is to phase-match the propagation constants of the fundamental modes of the capillaries forming the cladding to that of the unwanted higher mode of the core [10, 16, 17]. The LP_{11} in the core is thus coupled into the cladding and lost from the core. The desired fundamental core mode is not phase matched to any cladding modes and is unaffected, remaining low-loss. Here, we use the simple model of AR-HCF with the cladding made of circular capillaries to illustrate the general design principle of our approach. The effective refractive index of modes of a circular hollow waveguide can be estimated by Marcatilli and Schmeltzer's formula [19],

$$n_{eff} = 1 - \frac{1}{2}\left(\frac{V_{\nu m}\lambda}{2\pi r}\right)^2 \tag{1}$$

where λ is the wavelength, r is the radius of core, $V_{\nu m}$ is the m*th* zero root of first kind of Bessel function of $\nu - 1$ order.

In the case of a cladding made of circular capillaries, phase matching between LP_{11} mode of the core and fundamental modes of the air holes in the cladding requires that the ratio of their diameters D_{core}/D_{clad} should satisfy [17],

$$\frac{D_{core}}{D_{clad}} \sim \frac{3.832}{2.405} \approx 1.59 \tag{2}$$

#262357 Received 7 Apr 2016; revised 20 May 2016; accepted 27 May 2016; published 6 Jun 2016

This ratio is very far from achieved in the cladding lattice of PBG-HCFs or "Kagome" type HCFs, and although much closer, is still not achieved in our previous AR-HCF designs (see Fig. 1 ***left***). To reduce the ratio of D_{core}/D_{clad} in the fibers reported here we have reduced the number of capillaries in the cladding to seven which also reduces the absolute core diameter (Fig. 1 ***right*** and figures in Section 5).

3. Leakage loss measurement and mode excitation

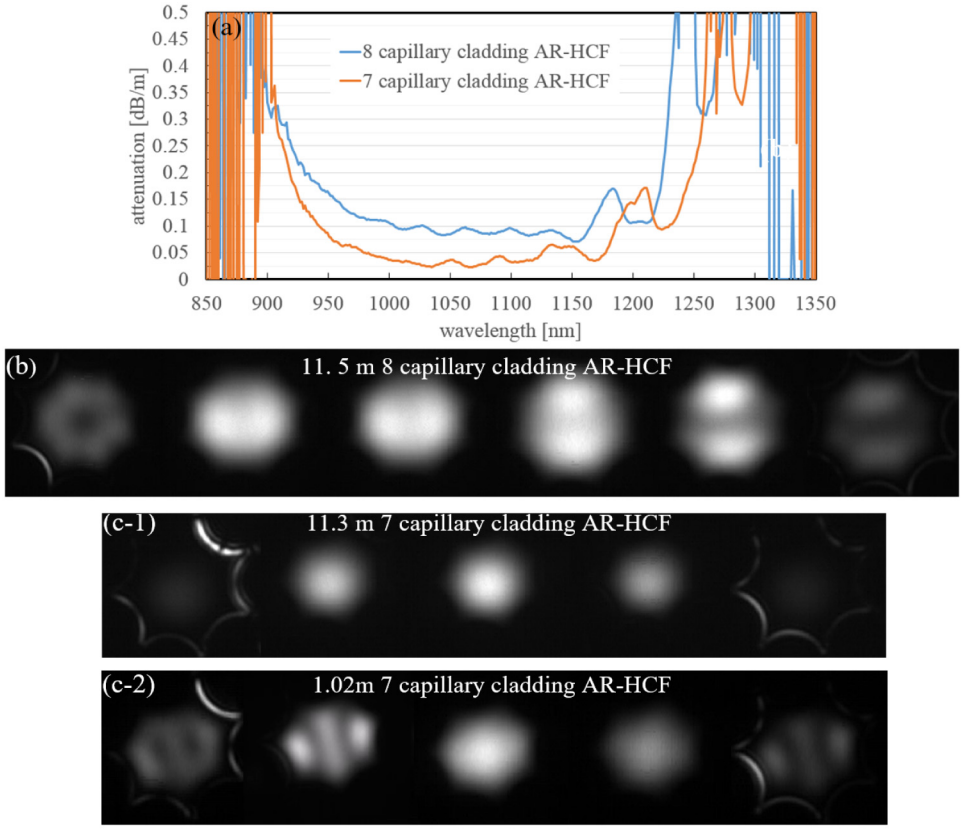

Fig. 2. (a) Measured attenuations of AR-HCFs by cut-back measurement. 8 capillary cladding AR-HCF was cut from 57.5 m to 20 m; 7 capillary cladding AR-HCF was cut from 45 m to 11.8 m. (b) Near field images of mode patterns at the output end of 11.5 m 8 capillary cladding AR-HCF under 1D input scan. (see Visualization 1). (c-1) and (c-2) Near field images of modes at the output end of 11.3 m and 1.02 m 7 capillary cladding AR-HCF under 1D scan. (see Visualization 2 and Visualization 3 respectively). The step of spatial scan is 5 μm. Due to the core size difference, fewer images are shown in (c-1) and (c-2).

Figure 2(a) shows the attenuation curves measured in the two fibers. Although we do not believe that bend loss is significant in the measurement [4], the fibers were rewound onto identical drums 31.8 cm in diameter to be certain that bend loss could not affect the comparison. The 8-capillary cladding AR-HCF was cut from 57.5 m to 20 m and the 7 capillary cladding AR HCF was cut from 45 m to 11.8 m. In the cutback measurements, the 8 capillary cladding AR-HCF had the near field images displaying a 'donut-like' pattern (Fig. 2(b)) at both lengths. A rich content of LP_{11} modes implies that the calculated attenuation reflects an average of both LP_{01} and LP_{11} modes. In contrast, only the fundamental mode was found in the cutback of the 7 capillary cladding AR-HCF. The minimum attenuation is below 0.025 dB/m around 1064 nm which is comparable to the previously-reported best figure of 0.026 dB/m at 1041 nm for a 32 μm core size in 8 capillary cladding AR-HCF [20]. There are

#262357 Received 7 Apr 2016; revised 20 May 2016; accepted 27 May 2016; published 6 Jun 2016

ripples in the attenuation curves of both fibers. We believe such features may be related to modes of the silica struts in the cladding.

Figures 2(b) and 2(c-1) are the near field images at the output of two AR-HCFs of similar lengths (11.5 m of 8 capillary AR-HCF and 11.3 m of 7 capillary AR-HCF) observed when scanning the input across the core. A conventional single-mode fiber with cut-off wavelength around 630 nm was used to butt-couple the input. A supercontinuum was used as a light source. The output end of the single-mode fiber was brought as close as possible to the input of the AR-HCF under test. The transverse position of the single-mode fiber was controlled by translation stages, and was scanned across the core diameter of the AR-HCF under test. The near field images of the output of the AR-HCFs were recorded by a CCD camera with a 10 nm bandpass filter centred at 1050 nm. Videos recording near field patterns of output of 7 capillary AR-HCFs of 1.02 m, 2.83 m and 5 m lengths under 1D scan of input can be found at Visualization 3, Visualization 4, and Visualization 5 respectively.

Figure 2(b) demonstrates the multimode transmission property of AR-HCFs with traditional 8 capillary cladding design. As the single-mode fiber moves further from the center, the modes of higher order are excited. Highly pure LP_{31} mode can be easily identified which implies low loss (the first image on the left of Fig. 2(b)).

In the 7 capillary AR-HCF, the misalignment of excitation only causes a change in intensity of LP_{01} mode in 11.3 m transmission (as shown in Fig. 2(c-1)). LP_{21}-like mode (as shown in Fig. 2(c-2)) can be observed when the length is cut to less than 3 m. By using off-center butt-coupling, a cutback measurement of LP_{21}-like modes confirms 2 dB/m attenuation at 1064 nm, which is nearly 100 times higher than measured for the LP_{01} mode. Note that even for 1 m fiber length, the 7-capillary fiber shows no evidence of LP_{11} mode transmission.

4. Demonstration of single-mode guidance by S^2 measurement

4.1 S^2 experiment

The spatially and spectrally (S^2) resolved imaging technique was first proposed by Nicholson et al for measuring mode contents of multimode solid fibers [21]. Later this technique was successfully applied in measuring the higher-order modes in PBG-HCF [22]. In this paper, we adopt S^2 measurement to confirm the mode contents of AR-HCFs.

Figure 3 illustrates the scheme of S^2 experiment. A supercontinuum light source was used as the optical source. Modes of the fiber under test were excited by using a lens. A standard single-mode fiber with cut-off wavelength at 920 nm was used to sample the spectra at the different positions on the near field image plane of the fiber output. The OSA resolution was set to 0.02 nm, which was the highest resolution achievable on the OSA.

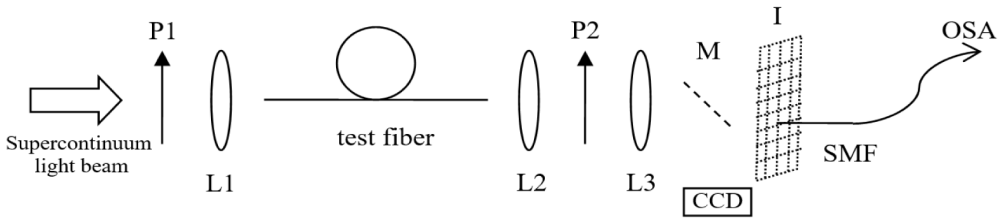

Fig. 3. Scheme of S^2 experiment. P1 and P2 are polarizers. L1, L2 and L3 are microscopic lenses. The near field image of output of test fiber is to project at imaging plane I. SMF is a single-mode fiber mounted on an X-Y translation stage rig and connected with OSA. OSA records spectra while SMF 2D scans at plane I under *LABVIEW* control. M is a flip mirror and a CCD camera is used to monitor the near field image at plane I.

4.2 Measurement results

Figure 4 shows the S^2 measurement results of two fibers. Both fibers were rewound in circles of over 1 m in diameter on bench. No extra bending was introduced.

#262357 Received 7 Apr 2016; revised 20 May 2016; accepted 27 May 2016; published 6 Jun 2016

The two fibers of similar lengths (11.5 m and 11.3 m) were excited in a similar fashion, to optimize the fundamental mode pattern at fiber outputs. The results are shown as the blu traces in Fig. 4. At the zero delay points (a) and (c), the reconstructed mode profiles are all the modes together. Since the fundamental mode in both fibers has a large proportion of the total power, the beam profiles both look like the LP_{01} mode. In the measurement of 8 capillary AR-HCF, a peak appears at a group delay of 1.35 ps/m with the amplitude 10 dB below zero delay, which matches precisely the prediction of Eq. (1) for the LP_{11} mode. Reconstruction of the modal intensity pattern at this delay (inset) suggests that this is indeed due to the modal interference between the LP_{11} mode and LP_{01} mode. However, the 7 capillary AR-HCF shown in Fig. 1(b) shows no significant peak at all in the S^2 measurement. No interference pattern due to LP_{21} modes was found around the 6 ps/m predicted by Eq. (1). To further demonstrate this single-mode performance, S^2 measurements at different wavelengths (990-994 nm, 1078-1082 nm and 1150-1154 nm) have been done and no higher-order mode peaks could be found.

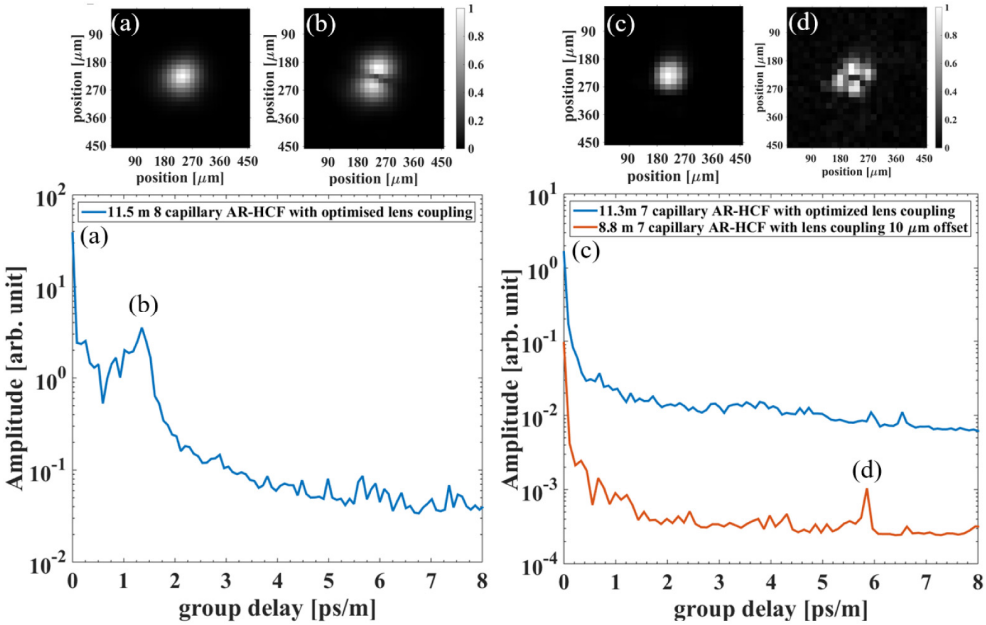

Fig. 4. S^2 measurement of AR-HCFs at the spectral window from 1078 nm to 1082 nm. Insets are the reconstructed mode profiles at different group delays. Left: 11.5m long 8-capillary cladding AR-HCF in the optimized coupling condition. The first peak at 1.352 ps/m (labelled "(b)") has the LP_{11} mode profile as shown on top. Right: Blue curve shows the measurement of 11.3m of 7-capillary cladding AR-HCF in the optimized coupling condition; Orange curve shows 8.8 m 7-capillary cladding AR-HCF in the offset coupling condition. No peak caused by the LP_{11} mode is found in the optimized or offset coupling conditions. In the 8.8 m length, the existence of LP_{21} mode is observed at 5.85 ps/m (labelled "(d)").

To explore the limit of single-mode performance of 7 capillary AR-HCF, S^2 measurements under different coupling conditions are studied. Using a slightly shorter fiber length of 8.8 m, we translated the input coupling lens off-center by 10 μm. We then observe a peak appearing at a delay of 5.85 ps/m as shown in Fig. 4(d) with amplitude nearly 20 dB below zero delay (the resolution of interference pattern of Fig. 4(d) is limited by the same spatial sampling rate and high rank higher-order mode in a smaller core size). This delay is consistent with excitation of the LP_{21} mode as predicted by Eq. (1) using the core diameter 26.3 μm. However, even this extreme misalignment does not result in any detectable interference peak caused by the LP_{11} mode near 2.53 ps/m as predicted by Eq. (1). This confirms the experimental demonstration of the LP_{11}-mode-free transmission in the 7 capillary cladding AR-HCFs.

#262357 Received 7 Apr 2016; revised 20 May 2016; accepted 27 May 2016; published 6 Jun 2016

5. Scaling of fibers for different wavelengths

We have drawn similar AR-HCFs for other shorter wavelengths. Figure 5 shows the measured attenuation of different single-mode AR-HCFs. Near field imaging indicates strongly single-mode performance in all fibers of approximate 10 m length. All the minimum attenuations shown in Fig. 5 are lower than any previously reported in their respective spectral windows [4]. SEMs of all five 7-capillary-cladding AR-HCFs can be found in [23].

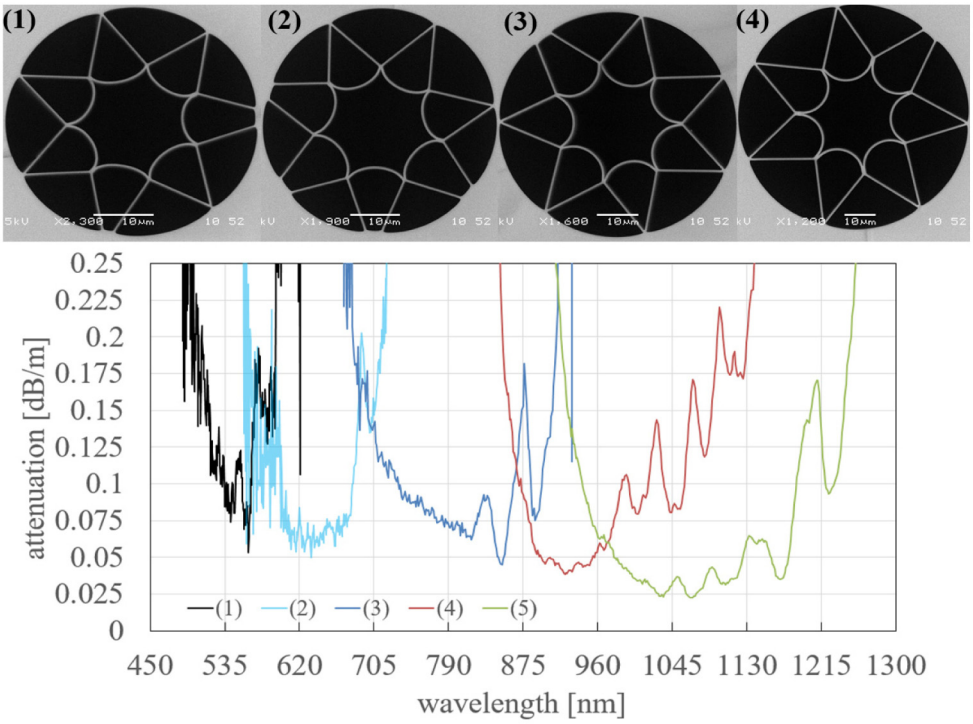

Fig. 5. Measured attenuation of single-mode AR-HCFs. Inset (1) to (4) are optical microscope images of AR-HCFs corresponding to the labelled attenuation curves. The attenuation curve of 7 capillary cladding AR-HCF in Fig. 2(b) is replotted as a reference. The minimum attenuations are 0.075 dB/m at 541 nm, 0.05 dB/m at 633 nm, 0.045 dB/m at 851 nm, 0.039 dB/m at 922 nm and 0.022 dB/m at 1068 nm.

6. Summary

In this paper, we compare two types of AR-HCFs and experimentally demonstrate the 7 capillary cladding AR-HCF with low-loss single-mode performance for a broad range of wavelengths. LP_{11}-mode-free transmission is experimentally demonstrated. The existence of LP_{21}-like modes in the transmission is confirmed with 2 dB/m attenuation through short fiber lengths. The scaling of fiber dimension of the new design verifies the robustness of low-loss single-mode guidance across the visible spectral range. All data underlying the results presented in this paper can be found at [23].

Acknowledgment

We acknowledge funding from the UK EPSRC under EP/M025381/1.

#262357 Received 7 Apr 2016; revised 20 May 2016; accepted 27 May 2016; published 6 Jun 2016